Journal of Fluorescence, Vol. 15, No. 4, July 2005 (© 2005)
DOI: 10.1007/s10895-005-2827-5

Water-Soluble Ln^{3+}-Doped LaF_3 Nanoparticles: Retention of Strong Luminescence and Potential as Biolabels

Peter R. Diamente[1] and Frank C. J. M. van Veggel[1,2]

Received November 1, 2004; accepted January 18, 2005

The use of optically robust, luminescent lanthanide-based particles is becoming an area of interest for biolabel-related chemistry, due to their long lifetimes and range of non-overlapping absorption and emission lines from the visible to the near-infrared. We report the synthesis and optical properties of water-soluble, luminescent Ln^{3+}-doped nanoparticles (NPs) coordinated with a hydrophilic $(RO)PO_3^{2-}$ ligand that facilitates the stabilization of the NPs in aqueous conditions, and that regulates particle growth to the nanometer range. The use of lanthanide ions as dopants, in particular Eu^{3+} and Er^{3+} ions, yields optically robust particles with narrow emission lines in the visible (591 nm) and in the near-infrared (1530 nm), respectively. Luminescent lifetimes range from the microsecond to the millisecond for Er^{3+} and Eu^{3+} ions, respectively, and the NPs are not expected to be susceptible to photobleaching due to the fact that the emissions arise from intra-4*f* transitions of the lanthanide ions.

KEY WORDS: Water-soluble nanoparticles; strong luminescence; lanthanide-doped lanthanum fluoride; near-infrared emission; biolabels.

INTRODUCTION

Nanomaterials constitute an emerging field in the chemical and materials sciences, due to the increasing interest in exploiting the luminescent properties of nanometer-sized materials. In particular, a very large interest in using nanoparticles (NPs) has developed due to their higher photo-stability and luminescence compared to organic dyes [1]. As a result, they are becoming highly favoured for biological applications such as bioconjugation due to their physical and optical properties [2].

Three types of NPs are commonly used as biological nanoprobes: latex nanospheres, luminescent quantum dots (QDs), and optically active metal NPs (such as gold or silver colloids) [3]. Of the three, QDs have been found significant use in biological applications, such as biological staining, diagnostics and fluorescence analysis, due to their high tunability of emission lines and their well established synthetic protocols which imparts water-soluble properties [4–7].

Of the many routes taken to impart biological activity to NP, bioconjugation of proteins to luminescent particles stabilized with derivatized poly(ethylene glycol) $[H(OCH_2CH_2)_nOH$, PEG] is among the most common. The biological advantage of covalently attaching NPs to biological macromolecules, such as peptided and proteins, with PEG chains (commonly referred to as PEGylation) is that it allows for suppression of antigenic and immunogenic epitopes, and prevents recognition and degradation by proteolytic enzymes [8,9]. Furthermore, the hydrophilic nature of PEG is an excellent ligand to render these NPs water soluble.

Here, we report the development of optically robust, water-soluble LaF_3-based NPs that are doped with Eu^{3+} and Er^{3+}, which are found to retain strong luminescence. The use of LaF_3-based NPs could have a number of advantages as probes used in bioconjugation over that of QDs. The optical properties seen for each lanthanide ion in the NP consists of non-overlapping absorption and emission lines that do not change position with particle

[1] Department of Chemistry, University of Victoria, P.O. Box 3065, Victoria, British Columbia, Canada V8W 3V6.
[2] To whom correspondence should be addressed. E-mail: FvV@uvic.ca

size, and thus do not interfere with the optical properties of other Ln^{3+} ions. Additionally, the inherent long-lived luminescent lifetimes (μs to ms range) prevents interference from any spontaneous background emission sources (natural fluorescence of proteins are within 1–10 ns [5]). Moreover, the spectroscopic selectivity of the NPs can be extended beyond the range of interferences from biological systems by means of doping with Er^{3+}, Nd^{3+}, Pr^{3+}, or Ho^{3+}, for near-infrared (NIR) emission lines [10–12]. Finally, the optical robustness of the NPs is due to the radiative transitions within the [Xe]4f^n configuration of the Ln^{3+} ions (the partially filled 4f orbitals are shielded from the environment by the filled 5s and 5p orbitals, minimizing the effects to the crystal field), resulting in long-term stability of the NP signal because there are no chemical bonds that can be broken in the photocycle [13].

The procedure used for NP synthesis utilized a water-soluble phosphate monoester-based ligand, $(RO)PO_3^{2-}$, which allowed for sub 20 nm particle formation in a single step under aqueous conditions, without the need to carry out subsequent reactions to impart water solubility. The Eu^{3+} ions have the advantage of being an ideal internal probe for spectroscopic studies due to its non-overlapping electric dipole (ED) ($^5D_0$-$^7F_{2,4,6}$) and magnetic dipole (MD) ($^5D_0$-$^7F_1$) transitions, which allow for qualitative analysis of the Eu^{+3} crystal field within the NP. In addition, NPs were also developed for potential biological applications by using the NIR emission lines of Er^{3+} ($^4I_{3/2}$-$^4I_{15/2}$ transition at 1530 nm), which allows for deeper signal depth penetration of tissue samples, NIR emission reduces the effects of tissue photon absorbance, absorption from water and blood (haemoglobin in particular), scatter, skin and adipose tissue refractive index mismatching as compared to the use of visible light [14,15]. Therefore, the use of a narrow emission line-based NPs, in conjunction with potentially biocompatible PEG-based ligands, gives us the first step towards bioconjugation of the NP.

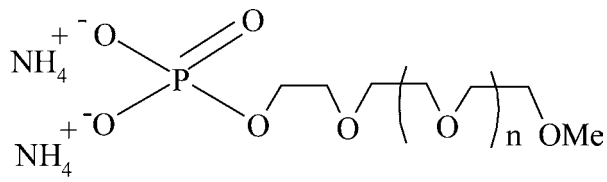

1·(2NH_4^+)

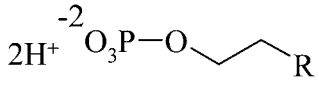

R = NH_2 for **2**·(2H^+), or
R = NHC(O)CH=CH_2 for **3**·(2H^+)

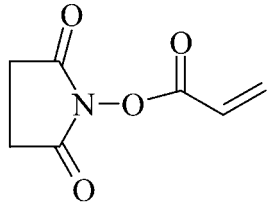

NASI

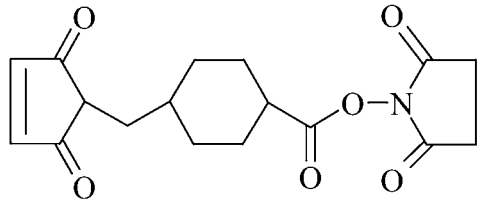

SMCC

Fig. 1. Ligands used.

RESULTS AND DISCUSSION

Synthesis

Six new water-soluble, highly luminescent NPs were prepared in a series of one-pot syntheses. Figure 1 shows the three ligands used for particle formation. The use of a PEG-based backbone for ligand **1**·(2NH_4^+) is due to the fact that PEG is know to be a hydrophilic ligand, which allows for the NP to be synthesized and analysed under aqueous conditions. The use of ligand **2**·(2H^+) was to demonstrate a proof-of-principle that with an amine-terminated ligand, the NP could be modified at the surface with *N*-acryloxysuccinimide (NASI), an activated ester-containing compound, and still retain both its physical and highly luminescent properties. All NPs synthesized were doped at 5 at.% of Eu^{3+} or Er^{3+} with respect to the total Ln^{3+} amount.

Synthesis of **1**·(2NH_4^+) was done by the reaction of the alcohol-terminated PEG-methyl ether with $OPCl_3$ under an inert environment, and isolated by diethyl ether extraction. The ^{1}H NMR spectrum of **1**·(2NH_4^+) after purification, shows the multiplet of the P—(OC**H**$_2$—R) linkage of the PEG unit to the phosphate at 4.0 ppm, which is further supported by ^{13}C NMR with the presence of

two doublets at 71.0 ppm P—(O—CH_2**C**H_2—R) and at 64.3 ppm (P—(O—**C**H_2CH_2—R), due to phosphate coupling. The ^{31}P NMR spectrum shows a singlet at 0.9 ppm (O_3**P**O—R) which is consistent with the expected range of phosphate monoesters.

The synthesis of the NP with ligand **1**·($2NH_4^+$) (referred to simply as **1**·LaF_3:Eu) was done by dissolving the ligand and NaF in water and THF (1:4 ratio v/v) followed by the addition of the Ln^{3+} salts. The resulting product was isolated from solution by precipitation and centrifuge, and purified by triturating. In previous work we have demonstrated that the ligands bind to the NP surface as anions and that the charge compensation is due to excess La^{3+} on the surface. NMR analysis of **1**·LaF_3:Eu gave the same peak locations as for the unbound ligand mentioned earlier, but they are heavily broadened due to the inhomogeneous distribution of the magnetic environment around the NP and a reduction in rotational freedom of the ligand [16,17]. Atomic force microscopy (AFM) of **1**·LaF_3:Eu showed a particle size distribution between 10–30 nm that is centred around 20 nm. All particles beyond 30 nm were not included in the histogram due to the effects of particle aggregation (refer to supplemental information for histogram, this information is available in pdf format upon request from the author).

Optical Properties of PEG-Based NP

Room temperature fluorescence excitation (λ_{em} 591 nm) and emission (λ_{ex} 397 nm) analysis of **1**·LaF_3:Eu, in H_2O, is shown in Fig. 2. The excitation spectrum shows the energy levels $^5D_4$ at 361 nm, $^5G_6$ at 376 nm, $^5G_2$ at 380 nm, $^5L_6$ at 397 nm, $^5D_3$ at 414 nm, and $^5D_2$ at 464 nm; the peak at 318 nm is unassigned due to the lack of information for that level. The emission spectrum shows the transitions $^5D_1$–$^7F_0$ at 525 nm, $^5D_1$–$^7F_2$ at 554 nm, $^5D_0$–$^7F_0$ at 578 nm, $^5D_0$–$^7F_1$ at 591 nm, $^5D_0$–$^7F_2$ at 613 nm, $^5D_0$–$^7F_3$ at 650 nm, and $^5D_0$–$^7F_4$ at 680–700 nm [11].

Qualitative information about the nature and symmetry of the Eu^{3+} ions is determined by analysing both the shape of the non-degenerate $^5D_0$–$^7F_0$ transition at 578 nm, and the $I^{^7F_2}/I^{^7F_1}$ intensity ratio, which is calculated to be 2.0 [18]. In comparing the $I^{^7F_2}/I^{^7F_1}$ intensity ratio of approximately 1 for bulk LaF_3:Eu NPs, the value of 2.0 for **1**·LaF_3:Eu is due to the fact that within the NP, the Eu^{3+} ions located near the surface experience a more asymmetric crystal field which increases the transition probability of the allowed electrical dipole ($^5D_0 \rightarrow {}^7F_2$ transition), resulting in an increase in its intensity [11,17,19]. Furthermore, due to the fact that the $^5D_0$ and $^7F_0$ states are non-degenerate, only a single gaussian-shaped peak for the transition should appear if all the Eu^{3+} ions are in the same crystal site. The enlarged high-resolution (0.05 nm) inset in Fig. 2 shows two peaks from the deconvolution of the 578 nm transition, indicating that the Eu^{3+} ions are located in more than one crystal site within the NP, which is consistent with the calculated $I^{^7F_2}/I^{^7F_1}$ intensity ratio.

The decay curve of the NP in H_2O, shown in Fig. 2, was excited at 464 nm collected at 591 nm to prevent any lifetime contributions from the $^5D_1$–$^7F_3$ level which overlaps the $^5D_0$–$^7F_2$ transition at 613 nm. Lifetime analysis was fitted with two exponentials, in which the longest lived component was 2.7 ms, followed by shorter lifetimes in the microsecond range (see Table I for full lifetime data), indicating that there are Eu^{3+} ions located in (at

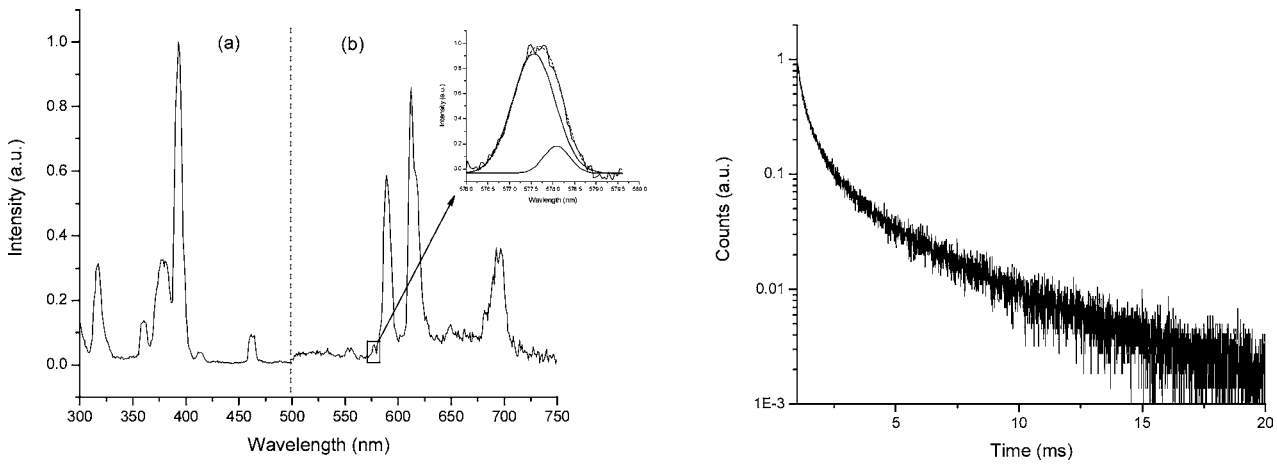

Fig. 2. *Left*: Excitation (a) and emission (b) spectra of **1**·LaF_3:Eu in H_2O. The inset shows the deconvolution of the high resolution (0.05 nm) 578 nm peak. The presence of two gaussian peaks is seen, indicating that the Eu^{3+} ions are located in more than one crystal site within the NP. *Right*: Decay curve of **1**·LaF_3:Eu in H_2O.

Table I. Decay Lifetimes

Compound	Solvent	τ_1	τ_2	τ_3
1·LaF_3:Eu at 5%	H_2O	2.7 ms (37%)	0.6 ms (34%)	0.2 ms (29%)
1·LaF_3:Er at 5%	D_2O	50 μs (45%)	11 μs (37%)	2 μs (22%)
2·LaF_3:Eu at 5%	H_2O	5.9 ms (50%)	2.5 ms (39%)	0.9 ms (11%)
2·LaF_3:Er at 5%	D_2O	118 μs (82%)	17 μs (17%)	—
2:**3**·LaF_3:Eu at 5%	H_2O	6.1 ms (54%)	2.3 ms (38%)	0.8 ms (8%)
2:**3**·LaF_3:Er at 5%	D_2O	50 μs (32%)	12 μs (43%)	3 μs (25%)
Surface reaction of **2**·LaF_3:Eu at 5% with NASI	H_2O	6.1 ms (53%)	2.5 ms (38%)	0.9 ms (9%)

least) two different crystal sites within the NP. The Eu^{3+} ions found within the "bulk" LaF_3 NP (those towards the centre of the core) give rise to the longest lifetimes due to minimal quenching sites, while those located near the surface are more susceptible to non-radiative quenching processes arising from surface-bound water molecules and high-energy ligand vibrations, thus reducing the luminescent lifetime [12].

Figure 3 shows the emission spectrum (λ_{ex} 488 nm) and decay curve of **1**·LaF_3:Er in D_2O (a weaker signal intensity was encountered when measured in H_2O), which the emission spectrum shows the expected transition at 1530 nm ($^4I_{13/2}$–$^4I_{15/2}$), while the analysis of the decay curve for the NP was fitted suitably with three exponentials, in which the longest lifetime is 50 μs. Despite the fact that Er^{3+} ions can have very long lived lifetimes, it is clear that there is still significant quenching in relation to the theoretical lifetime of up to 20 ms [20]. The effects of surface-related quenching effects can be reduced by the formation of core-shell NPs, where the growth of a layer of LaF_3 around the core minimizes contact between the dopant ions and sources of non-radiative quenching processes [17]. Refer to Table I for full luminescence lifetimes.

Analysis of NPs with 2-Aminoethyl Dihydrogen Phosphate (2·($2H^+$))

Synthesis of **2**·LaF_3:Eu was done in order to study the spectroscopic effects of amine-terminated ligands on the NP. The nature of the ligand **2**·($2H^+$) is intended as a proof-of-principle that the surface-bound ligands can be reacted with an activated ester. Synthesis of the NPs was done by dissolving **2**·($2H^+$) in water at 37°C, neutralizing with NH_4OH, followed by the addition of NaF and the Ln^{3+} salts. The NPs were precipitated with acetone and isolated by centrifuge.

Characterization of the NP was done by NMR (^{1}H, ^{13}C, ^{31}P) and fluorescence analysis. The ^{1}H NMR spectrum of **2**·LaF_3:Eu shows the two C**H**$_2$ peaks located at 4.0 and 3.2 ppm, and the ^{13}C NMR spectrum shows peaks at 40.5 ppm (—OCH_2**C**$H_2NH_3^+$) and 60.8 ppm (—O**C**$H_2CH_2NH_3^+$), all broadened as expected. The ^{31}P

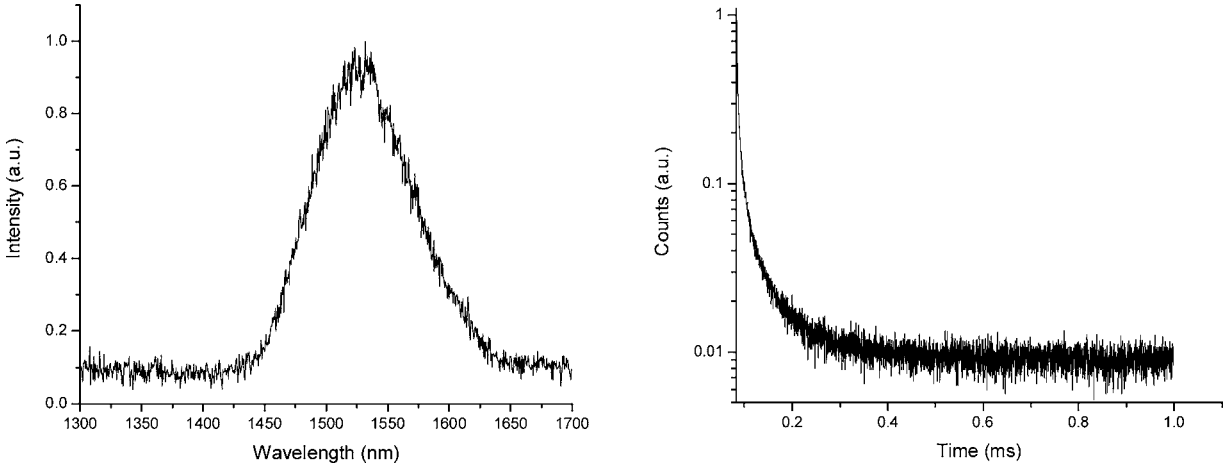

Fig. 3. *Left*: Emission spectrum of **1**·LaF_3:Er in D_2O. *Right*: Decay curve of **1**·LaF_3:Er in D_2O.

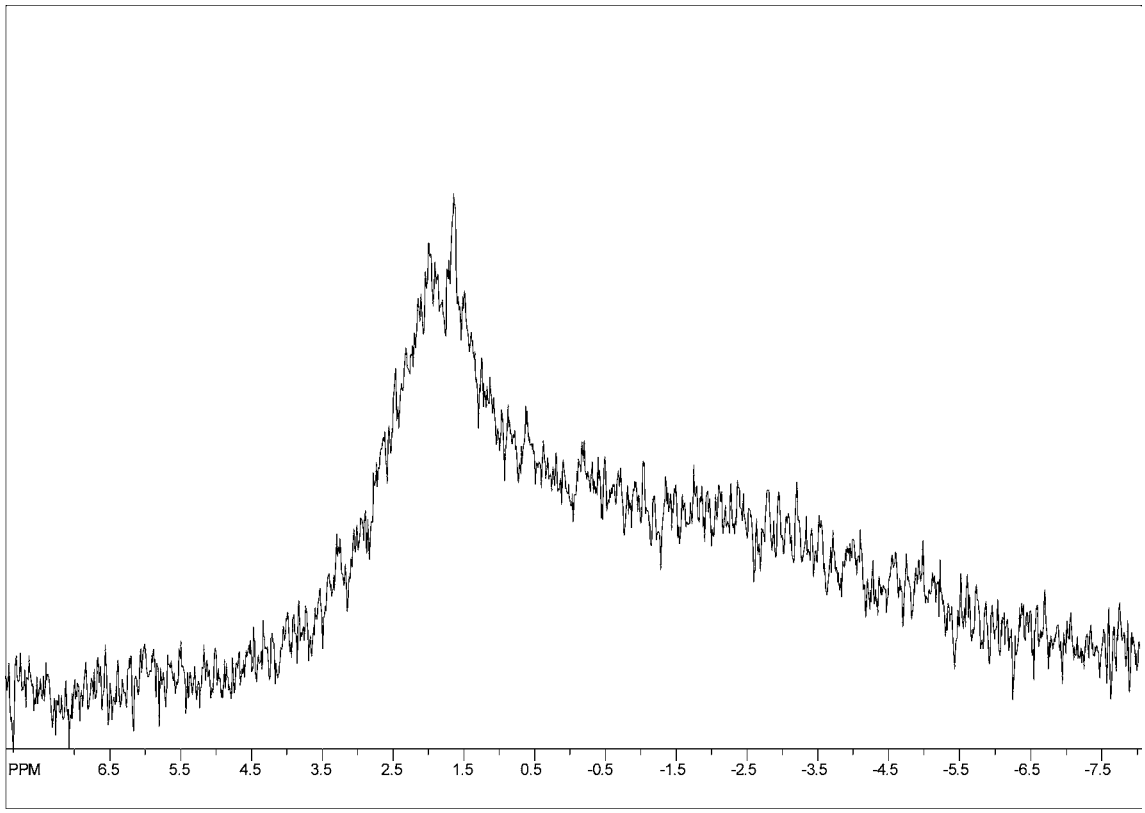

Fig. 4. ^{31}P NMR of **2**·LaF_3:Eu in D_2O.

NMR spectrum in Fig. 4 shows a broad peak (1.5 ppm) overlapping a very broad peak (4.0 to −6.0 ppm), apparently arising from different coordination dynamics of the ligands on the surface of the NP. That is, the broad peak at 1.3 ppm is due to restricted rotation of the ligand on the NP, and the very broad peak arises from even more restricted rotation at a different location on the NP. This is consistent with the line broadening effects seen with core-shell NPs in other work from us, where a shell of LaF_3 is grown around the LaF_3:Eu core, which seems to rule out the effect of the paramagnetic Eu^{3+} as the cause [17].

Figure 5 shows the emission spectrum and decay curve (in H_2O) of **2**·LaF_3:Eu. As can be seen, the expected Eu^{3+} peaks are present, in which the enlarged area at 578 nm can be fitted with two gaussian peaks overlapping each other, arising from Eu^{3+} ions present in both the bulk and near or on the surface of the NP (*supra vide*). As before, the 612 nm peak dominates the emission spectrum ($I^{^7F_2}/I^{^7F_1}$ ratio of 1.5) indicating that the Eu^{3+} ions located near the surface of the NP are in a more asymmetric crystal field, similar to **1**·LaF_3:Eu. The decay curve was fitted with three exponentials with lifetime values of 5.9, 2.5, and 0.9 ms, which is consistent with Eu^{3+} ions being located in different crystals sites within the NP. In relation to **1**·LaF_3:Eu, the shorter lifetimes measured are likely a result of reduced ligand loading on the surface of the NP, increasing the amount of possible quenching groups, in particular H_2O, on the surface of the NP [19]. The fact that the decay curve for **2**·LaF_3:Eu was fitted with three lifetimes and the 578 nm peak was deconvoluated into two gaussian curves is not necessarily in contradiction. By coincidence, emission peaks of the $^5D_0$ to $^7F_0$ might overlap and additionally the flank of the 590 peak made base line correction not very accurate, which resulted in physically unrealistic gaussians when three were tried.

To test the near-infrared (NIR) luminescent capabilities of the particles, synthesis of **2**·LaF_3:Er was carried out in which the emission spectrum, in D_2O, shows the same $^4I_{3/2}$–$^4I_{15/2}$ transition at 1530 nm seen for **1**·LaF_3:Er. The decay curve was fitted with two exponentials yielding lifetime values of 118 μs (82%) and 17 μs (17%), which is within range of **1**·LaF_3:Er, indicating that the Er^{3+} ions are still significantly quenched by solvent and ligand interactions. Improvement of the luminescent lifetimes can be achieved by forming core-shell NPs, thus reducing solvent quenching effects (*supra vide*).

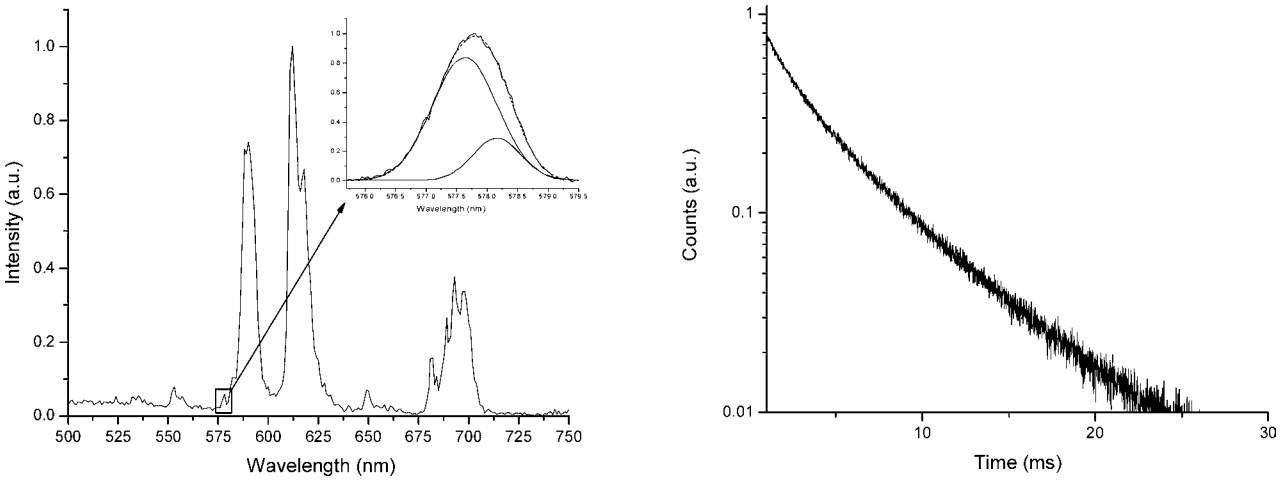

Fig. 5. *Left*: Emission spectrum of **2**·LaF_3:Eu in H_2O. The inset shows the deconvolution of the high-resolution (0.05 nm) 578 nm peak. *Right*: Decay curve of **2**·LaF_3:Eu in H_2O.

To test the ability of **2**·LaF_3:Eu to be reacted with a model compound of a heterobifunctional cross-linking unit (typically used for bioconjugation reactions), the ligand **2**·($2H^+$) was reacted with an activated ester, NASI, yielding an acrylamide-terminated ligand. First, we tested the synthesis of the NPs (method **A**) with a ligand mixture of **2**·($2H^+$) and **3**·($2H^+$) at a 1:0.2 molar ratio (a molar ratio beyond 1: 0.5 resulted in a significant decrease in NP solubility due to the larger number of vinyl-terminated ligands). The ^{1}H NMR gave the expected broad peaks seen for **2**·LaF_3:Eu, in addition to the broad vinyl acrylamide peaks at 6.2 and 5.8 ppm. Removal of **2**·($2H^+$) and **3**·($2H^+$) to estimate the molar ratio of the ligands on the surface of the NP was accomplished by adding 0.3 mL of citrate buffer solution (buffer pH $\sim$ 6) to the NMR tube, and letting it sit for 2 days. The resulting ^{1}H NMR ratio of the ligand mixture **2**·($2H^+$) and **3**·($2H^+$) was calculated to be approximately 20%, which is in accordance to what was expected due to the fact that both ligands are linear structures in solution, resulting in minimal steric hindrance of the two ligands after surface coordination (refer to supplemental information). The ^{31}P NMR analysis showed a broad peak at 1.3 ppm overlapping an even broader peak from 4.0 to -6.0 ppm, similar to **2**·LaF_3:Eu.

The second method tested (method **B**) involved the surface reaction of NASI with **2**·LaF_3:Eu. The ^{1}H NMR of the NPs show the same peak positions and line broadening as those from method **A**, indicating that the surface reaction was successful. Calculation of the amount of NASI reacted on the surface was not carried out, but is expected to be in excess of 50% due to the significant decrease in product solubility. Surface concentration of acrylamide can be controlled by varying the amount of NASI used in the reaction.

Analysis of the overlaid emission spectra in Fig. 6 of the NPs from method **A** and **B** show the same $I^{^7F_2}/I^{^7F_1}$ intensity ratio of 1.6, with the enlarged area at 578 nm showing identical asymmetrical peaks. The decay curves for the both methods were fitted with three exponentials, which were within experimental error ($\pm$5% in duplicate) of the unreacted **2**·LaF_3:Eu, further demonstrating that the ligand mixture of **2**·($2H^+$) and **3**·($2H^+$) does not alter the NP synthesis. Synthesis of the NPs doped with Er^{3+} by method **A** shows the expected Er^{3+} $^4I_{3/2}$–$^4I_{15/2}$ transition peak at 1530 nm, with a decay curve that was fitted with three exponentials, yielding lifetime values of 50 μs (32%), 12 μs (43%), and 3 μs (25%).

Current research focuses on the reaction of the amino group on the surface of the NPs with heterobifunctional cross-linkers, such as SMCC (Fig. 1), followed by the Michael addition of a thiol group from cysteine, antibodies, etc. Preliminary results show that the reaction of the heterobifunctional cross-linker biotin-NHS yields spectroscopic data that are identical to those of the acrylamide-based NPs, demonstrating the versatility and stability of the NP. In addition, we are developing PEG-based ligands that have a terminal amino group.

CONCLUSION

A one-step synthesis of optically robust, water-soluble Ln^{3+}-doped LaF_3 NPs was achieved through the use of the $(RO)PO_3^{2-}$ coordinating unit with PEG-based and $(CH_2)_2NH_2$-terminated ligands. The synthesis

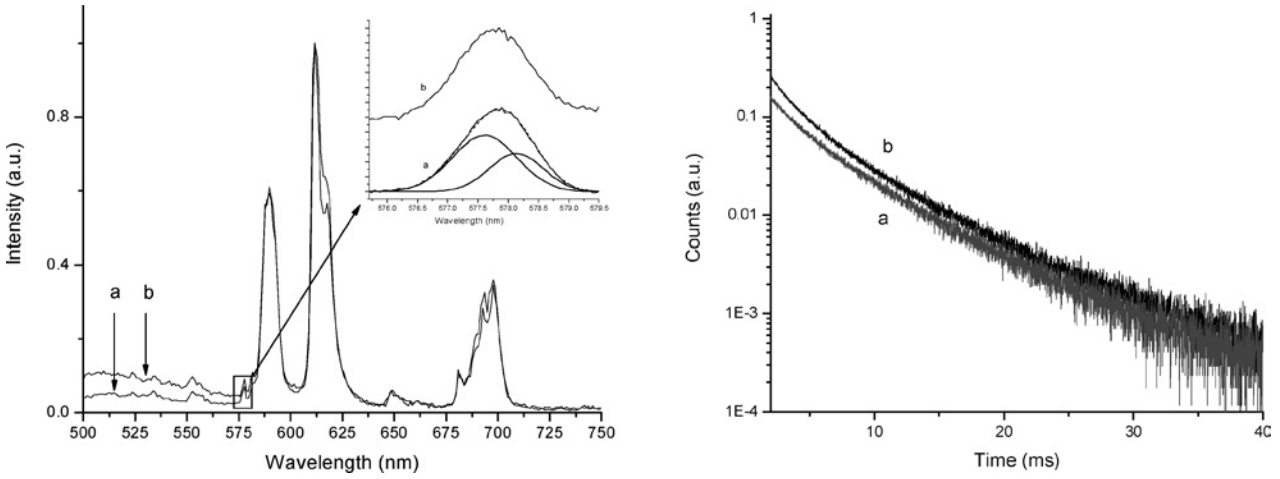

Fig. 6. *Left*: Overlaid emission spectra of surface reacted **2**·LaF_3:Eu with NASI (line a), and **2**:**3**·LaF_3:Eu (line b). The spectra are offset for clarity. The inset shows the deconvolution of the high-resolution (0.05 nm) 578 nm peak. *Right*: Overlaid decay curves of surface reacted **2**·LaF_3:Eu with NASI (line a), and **2**:**3**·LaF_3:Eu (line b). The curves are offset for clarity.

demonstrated that the NPs can be doped with Eu^{3+} and Er^{3+} ions, which exhibited strong luminescence in the visible (300–750 nm) and NIR (1450–1600 nm) region, respectively, under aqueous conditions. Analysis of the emission spectra showed that the Eu^{3+} ions are located in more than one crystal site due to the asymmetry of the 578 nm emission, which was further supported by the multi-exponential decay of the Eu^{3+}-doped NPs, which is in full agreement with earlier work. The lifetime values calculated were in the millisecond range for Eu^{3+}-doped NPs, and in the 50–100 μs range for Er^{3+}-doped NPs.

The use of amine-terminated ligands for NP formation allowed for proof-of-principle that the NPs can be reacted with an activated ester (*N*-acryloxysuccinimide) while still retaining a high level of water solubility and luminescence. This was demonstrated by the consistent I^{7F_2}/I^{7F_1} intensity ratio of the 591 and 612 nm peaks, similar multi-exponential lifetimes, and peak deconvolution of the non-degenerate 578 nm transition, clearly showing that the spectroscopic properties of the reacted NPs were unaffected by the surface reactions.

EXPERIMENTAL

All chemicals were obtained from Aldrich and used without further purification unless otherwise indicated. All sources of water used consisted of distilled water. All NPs were made with LaF_3 at 5% Eu^{3+} or Er^{3+} atom doping on the total Ln^{3+} amount. All steady-state fluorescence analyses were done using an Edinburgh Instruments FLS 920 fluorescence system, which was equipped a 450 W xenon arc lamp via a M300 single grating monochromator. A red-sensitive peltier-cooled Hamamatsu R955 photomultiplier tube (PMT), with a photon-counting interface, was used for analyses between 200 and 850 nm, and a N_2-cooled Hamamatsu R5509 PMT was used for analyses between 400 and 1700 nm. All emission and excitation analyses in the visible region were measured with a 1 nm resolution, or 0.05 nm for high-resolution analyses, and NIR emission analyses were done with a 5 nm resolution. Lifetime analyses were done by exciting the solutions with a 10 Hz Quantel Brilliant Q-Switch (optical range from 409 to 2400 nm) pumped by a Nd:YAG laser and collecting the emission using the respective detectors mentioned earlier. Decay curves were measured with a 0.2 and a 0.01 ms lamp trigger delay for the R955 and R5509 PMT, respectively. All lifetime analyses were calculated using the Edinburgh Instruments F900 software and signal intensities greater than 1% of the maximum intensity were included, and were fitted so as to obtain χ^2 values from 1.0 to 1.3. If two exponentials did not give an acceptable fit, three exponentials were taken. Reported lifetime and percent contribution are only treated in a qualitative sense, and errors were estimated to be 5% based on duplicate measurements. Peak deconvolution was done using software from Originlab (Origin 7.5). All ^1H and ^{13}C NMR analysis was done using a Bruker 300 MHz NMR instrument, and ^{31}P NMR was done on a Bruker AMX 350 MHz instrument. Chemical shifts of ^{31}P NMR were measured relative to an external standard of 85% H_3PO_4. No NMR analysis was carried out on Er^{3+}-based NP due to severe line broadening. Atomic force microscopy was done using a Thermomicroscope Explorer AFM instrument with contact-mode analysis on freshly cleaved mica: sample deposition was done by spin coating at 2000 rpm from a

water suspension. The particle size distribution was based on 265 particles.

1·2NH_4^+: A solution of 10.5 g (18.5 mmol) poly(ethylene glycol) methyl ether (ca. M_n 550) with molecular sieves was stirred overnight to remove residual water. Then 20 mL of anhydrous THF (distilled from Na^+/benzophenone) was added, and slowly dropped to $OPCl_3$ (1.42 g, 9.2 mmol) at −15°C under Ar. The solution was slowly allowed to warm to room temperature and stirred for 2 h, followed by the addition of 1 mL of water and vigorous stirring for 1 h. Subsequently, 100 mL of ethyl acetate was added and the organic layer was extracted, dried over $MgSO_4$, and evaporated to dryness. Finally, 20 mL of hexane was added and NH_3 was bubbled through the solution. The solvent was removed by rotary-evaporation, and then dried. The product was triturated in methanol and THF, and isolated by centrifuge. A white semi-solid remained. Impurities due to unreacted PEG are present at less than 5%, and the inorganic phosphate is a result of phosphate hydrolysis. ^{1}H NMR: δ (D_2O): 3.9 (dt, $^3J_{HP}$ = 8.1 Hz, $^3J_{vic}$ = 6.4 Hz, 2H, P—(OC**H**$_2$—)), 3.8–3.4 (m, 49H, (—C**H**$_2$OC**H**$_2$—)$_n$ of the PEG), 3.4 (s, 3H, —OC**H**$_3$); ^{13}C NMR: δ (D_2O): 71.0 (d, $^3J_{CP}$ = 7.9 Hz, P—(O—CH_2**C**H_2—O—R)$_2$), 69.8 (m, (CH_2—O—**C**H_2)$_n$), 64.3 (d, $^2J_{CP}$ = 5.5 Hz, (P—(O—**C**H_2CH_2—R)$_2$), 58.7 (s, R—O—**C**H_3); ^{31}P NMR: δ (D_2O): 0.9 (s, O_3**P**O—R).

1·LaF_3:Eu: At room temperature, a solution of **1**·(2NH_4^+) (1.15 g, 0.95 mmol) was dissolved in 30 mL of THF and stirred for 15 min, followed by the addition of NaF (0.13 g, 3.00 mmol) in 7 mL of H_2O. The solution was stirred for 15 min followed by the drop-wise addition of $La(NO_3)_3$·$6H_2O$ (0.54 g, 1.26 mmol) and $Eu(NO_3)_3$·$5H_2O$ (0.03 g, 0.04 mmol) in 2 mL of H_2O. The suspension was stirred for 1 h, and then the solvent was removed by rotary-evaporation, and then dried overnight under reduced pressure. The product was then triturated with 20 mL of THF (a loose white suspension formed), separated by centrifuge, and then washed and separated with THF three times. The final product was a white, highly water-soluble powder. Some hydrolysed phosphates, as inorganic phosphate and polyphosphates, were present but did not impede with NP formation. ^{1}H NMR: δ (D_2O): 4.0 (bs, 2H, POC**H**$_2$—), 3.7 (bs, 54H, —C**H**$_2$—O—C**H**$_2$—), 3.4 (s, 3H, —C**H**$_3$); ^{31}P NMR: δ 0.9 (s, O_3**P**O—R).

1·LaF_3:Er: The same method was used as described earlier, but with $Er(NO_3)_3$·$5H_2O$ (0.03 g, 0.27 mmol).

2·LaF_3:Eu: A solution of **2**·(2H^+) (0.14 g, 1.02 mmol) in 25 mL of water was neutralized with NH_4OH, followed by the addition of NaF (0.13 g, 3.00 mmol). The solution was heated to 37°C, and then added to it was a solution of $La(NO_3)_3$·$6H_2O$ (0.54 g, 1.26 mmol) and $Eu(NO_3)_3$·$5H_2O$ (0.03 g, 0.04 mmol) in 2 mL of water. The solution was added drop-wise and stirred at 37°C for 16 h, yielding a clear solution. Isolation of the particles was done by removing the water until the product was reduced to a paste-like consistency, then redissolved with 5 mL of water and precipitated with acetone. The particles were then isolated by centrifuge, and the supernatant poured off, and the remaining precipitate was then triturated with acetone, separated by centrifuge, and dried under reduced pressure. ^{1}H NMR: δ (D_2O): 4.0 (bs, 2H, POC**H**$_2CH_2NH_3^+$), 3.7 (bs, 2H, $POCH_2$C**H**$_2NH_3^+$); ^{13}C NMR: δ (D_2O): 61.0 (bs, $POCH_2$**C**$H_2NH_3^+$), 40.0 (bs, PO**C**$H_2CH_2NH_3^+$); ^{31}P NMR: δ (D_2O): 1.3 (bs, O_3**P**O—R) and −1.5 (very bs, O_3**P**O—R). For comparison, the NMR data for **2**·(2H^+) are given here as well; ^{1}H NMR: δ (D_2O): 4.1 (dt, $^3J_{HP}$ = 7.1 Hz, $^3J_{vic}$ = 5.7 Hz, 2H, POC**H**$_2CH_2NH_3^+$), 3.7 (t, $^3J_{vic}$ = 5.7 Hz, 2H, $POCH_2$C**H**$_2NH_3^+$); ^{13}C NMR: δ (D_2O): 61.1 (d, $^2J_{CP}$ = 5.0 Hz, $POCH_2$**C**$H_2NH_3^+$), 40.2 (d, $^3J_{CP}$ = 8.2 Hz, PO**C**$H_2CH_2NH_3^+$); ^{31}P NMR: δ (D_2O): 0.4 (s, O_3**P**O—R).

2·LaF_3:Er: same method as described earlier, but with $Er(NO_3)_3$·$5H_2O$ (0.03 g, 0.27 mmol).

3·(2H^+): In 4 mL of water at 37°C, **2**·(2H^+) (0.14 g, 1.0 mmol) was added, neutralized with NaOH (aq) to a pH of ∼7, followed by the addition of NASI (0.27 g, 1.6 mmol) dissolved in four drops of DMSO. The reaction was stirred for 1 h at 37°C. Separation was carried out by extracting the impurities with 20 mL of diethyl ether, isolating the aqueous phase, removing the water by rotary-evaporation at 80°C, and drying overnight under reduced pressure. The isolated product was a white solid. Some *N*-hydroxysuccinimide and hydrolysed phosphates was present. ^{1}H NMR: δ (D_2O): 6.4 – 6.1 (m, 2H, —C**H**$_a$=C**H**$_{b,c}$), 5.7 (dd, $^3J_{cis}$ = 10.3 Hz, $^2J_{gem}$ = 1.5 Hz, 1H, —CH=C**H**$_{c,b}$), 3.8 (dt, $^3J_{HP}$ = 6.6 Hz $^3J_{gem}$ = 5.9 Hz, 2H, OC**H**$_2CH_2NH$—), 3.4 (t, $^3J_{gem}$ = 5.9 Hz, 2H, —OCH_2C**H**$_2$NH—); ^{13}C NMR: δ (D_2O): 177.6 (s, H_2C=CH—**C**O—N), δ 130.4 (s, H_2**C**=CH—), 127.8 (s, H_2C=**C**H—), 63.2 (d, $^2J_{P-C}$ = 5.5 Hz, $POCH_2$**C**H_2NRH), 40.3 (d, $^3J_{P-C}$ = 6.8 Hz, PO**C**H_2CH_2NRH), 25.6 (s, —CO(**C**H_2)$_2$CO—); ^{31}P NMR: δ (D_2O): 0.6 (s, O_3**P**O—R).

2·(2H^+):**3**·(2H^+) at 1:0.2 molar ratio: In 4 mL of water at 37°C, **3**·(2H^+) (0.14 g, 1.0 mmol) was added, neutralized with $NaOH_{(l)}$ to a pH of ∼7, followed by the addition of NASI (0.03 g, 0.2 mmol) in four drops of DMSO. The reaction was stirred for 1 h at 37°C. Separation was carried out by extracting with 20 mL of ether, isolating the aqueous phase, removing the water by rotary-evaporation at 80°C, followed by overnight drying under reduced pressure. The isolated mixture was a

white solid. Refer to **3**·($2H^+$) and **2**·LaF_3:Eu for NMR assignments.

2:**3**·LaF_3:Eu: NP synthesis followed the same procedure used for **2**·LaF_3:Eu, but with a mixture of **2**·($2H^+$) and **3**·($2H^+$) at 1:0.2 molar ratio. ^{1}H NMR: δ (D_2O): 6.2 (bs, C**H**$_a$═C**H**$_{b,c}$), 5.8 (bs, CH$_a$═C**H**$_{c,b}$—), 4.0 (bs, OC**H**$_2$CH$_2$N—), 3.2 (bs, OCH$_2$C**H**$_2$N—); ^{31}P NMR: δ (D_2O) 1.3 (bs, O_3**P**O—R) and −1.5 (very bs, O_3**P**O—R).

2:**3**·LaF_3:Er: Same procedure as described earlier, but with $Er(NO_3)_3{\cdot}5H_2O$ (0.03 g, 0.27 mmol).

Surface reaction of **2**·LaF_3:Eu with NASI: In 4 mL of H_2O, **2**·LaF_3:Eu (0.1 g) was dissolved in water and heated to 37°C under constant stirring, followed by the addition of NASI (7.1 mg, 0.04 mmol) dissolved in four drops of DMSO. Separation was carried out by extracting the impurities with 20 mL of ether, isolating the aqueous phase, and removing the water by rotary-evaporation until a paste-like consistency remained. The product was purified by dissolving in 2 mL of water followed by the addition of acetone to form a precipitate, isolated by centrifuge, and dried under reduced pressure. ^{1}H NMR: δ (D_2O): 6.2 (bs, C**H**$_a$═C**H**$_{b,c}$), 5.8 (bs, CH═C**H**$_{c,b}$), 4.0 (bs, OC**H**$_2$CH$_2$N—), 3.2 (bs, CH$_2$C**H**$_2$N—).

REFERENCES

1. Z. Ye, M. Tan, G. Wang, and J. Yuan (2004). *J. Mater. Chem.* **14**, 851–856.
2. X. D. Hai, M. Q. Tan, G. Wang, Z. Q. Ye, J. L. Yuan, and K. Matsumoto (2004). *Anal. Sci.* **20**, 245–246.
3. C. Sun , J. Yang , L. Li , X. Wu , Y. Liu, and S. Liu (2004). *J. Chromatogr. B* **803**, 173–190.
4. J. M. Tsay, M. Pflughoefft, L. A. Bentolila, and S. Weiss (2004). *J. Am. Chem. Soc*. **126**, 1926–1927.
5. M. Tan, Z. Ye, G. Wang, and J. Yuan (2004). *Chem. Mater*. **16**, 2494–2498.
6. Z. F. Li and E. Ruckenstein (2004). *Nano Lett*. ***8***, 1463–1467.
7. D. Wang, A. L. Rogach, and F. Caruso (2002). *Nano Lett*. **8**, 857–861.
8. M. J. Roberts, M. D. Bentley, and J. M. Harris (2002) *Adv. Drug Deliv. Rev.* **54**, 459–476.
9. A. M. Derfus, W. C. W. Chan, and S. N. Bhatia (2004). *Adv. Mater*. **12**, 961–966.
10. G. A. Hebbink, J. W. Stouwdam, D. N. Reinhoudt, F. C. J. M. van Veggel (2002). *Adv. Mater.* **16**, 1147–1150.
11. J. W. Stouwdam and F. C. J. M. van Veggel (2002). *Nano Lett*. **7**, 733–737.
12. K. Driesen, R. Van Deun, C. Görller-Walrand, and K. Binnemans (2004). *Chem. Mater*. **16**, 1531–1535.
13. S. I. Klink, G. A. Hebbink, L. Grave, P. G. B. Oude Alink, F. C. J. M. van Veggel, and M. H. V. Werts (2002). *J. Phys. Chem.* A **15**, 3681–3689.
14. D. R Larson, W. R. Zipfel, R. M. Williams, S. W. Clark, M. P. Bruchez, F. W. Wise, and W. W. Webb (2003). *Science* **300**, 1434–1436.
15. Y. T. Lim, S. Kim, A. Nakayama, N. E. Stott, M. G. Bawendi, and J. V. Frangioni (2003). *Mol. Imag.* **1**, 50–64.
16. J. W. Stouwdam and F. C. J. M. van Veggel (2004). *Langmuir* **20**, 11763–11771.
17. V. Sudarsen, F. C. J. M. van Veggel, R. A. Herring, M. Raudsepp (2005). *J. Mater. Chem.* **15,** 1332–1342.
18. M. H. V. Werts, R. T. F. Jukes, and J. W. Verhoeven (2002). *Phys. Chem. Chem. Phys.* **4**, 1542–1548.
19. J. W. Stouwdam, G. A. Hebbink, J. Huskens, F. C. J. M. van Veggel (2003). *Chem. Mater.* **15**, 4604–4616.
20. M. J. A. de Dood, L. H. Slooff, A. Polman, A. Moroz, A. van Blaaderen (2001). *Appl. Phys. Lett*. **22**, 3585–3587.